Yield Estimation of Paddy in Bhandara District, Maharashtra, India, Using a Semi-Physical Remote Sensing Approach

ABSTRACT:

Accurate and early estimation of crop yield is essential for food security planning, market regulation, and sustainable resource management. This study applies a semi-physical remote sensing approach to estimate paddy yield in Bhandara District, Maharashtra, India, for the 2018-2022 kharif seasons. Satellite-derived Photosynthetically Active Radiation (PAR), Fraction of Absorbed PAR (fAPAR), Radiation Use Efficiency (RUE), temperature stress, and water stress were integrated into a Net Primary Productivity (NPP) model to generate spatially explicit yield maps. A paddy crop mask was prepared from Sentinel-2 data, while MODIS and INSAT-3D products provided biophysical inputs. Grain yield was obtained by applying a harvest index to NPP estimates. Validation against five-year crop-cutting statistics showed an overall mean deviation of -1%, indicating close agreement between remote sensing estimates and official records. The results confirm that combining simplified process-based modeling with satellite data can provide reliable and timely yield forecasts over heterogeneous agricultural landscapes. This methodology supports decision-making for farmers, planners, and policymakers, and offers potential for operational yield monitoring in other rice-growing regions.

Keywords:

Rice yield, Remote Sensing, Net Primary Productivity, Semi-physical model, MODIS, Bhandara District

1. INTRODUCTION:

Rice is one of the most important cereal crops worldwide, supplying calories to more than half of the global population and acting as a cornerstone of food and livelihood security in Asia (Ma et al., 2018). In India, rice plays a particularly critical role in ensuring food security for an ever-growing population. With 43.86 million hectares under cultivation and a production of approximately 130.29 million tonnes in the fiscal year 2021–2022, the country stands as the world's second-largest rice producer and a leading exporter (Ma et al., 2018). Yet, despite these notable achievements, India's average rice productivity remains comparatively low relative to many other rice-producing nations, largely due to climatic variability, water scarcity, soil degradation, and sub-optimal agronomic practices (Jia et al., 2020; Ma et al., 2018). Enhancing yield and developing robust forecasting systems are therefore essential to meet the rising demand, sustain food availability, and strengthen procurement and trade policies (Pan et al., 2011).

Rice cultivation in India occurs across a diverse range of climatic zones and soil types, encompassing the northeastern states (Assam, Arunachal Pradesh, Manipur), the eastern region (Odisha and West Bengal), the northern plains (Punjab and Uttar Pradesh), western areas such as Maharashtra and Gujarat, and the southern tip including Tamil Nadu and Andhra Pradesh. More than 60% of India's population depends heavily on rice as a staple food, underlining the need for consistent and reliable production to support national food security.

Accurate estimation of crop yields supports not only food security but also market stability, irrigation scheduling, and the development of early warning systems (Beer et al., 2010; Potter et al., 1993). Traditional yield assessment techniquessuch as crop-cutting experimentsremain important for ground truthing but are expensive, labour-intensive, and limited in their spatial coverage (Bégué et al., 2010). In recent decades, Earth-observation technology has emerged as a cost-effective and powerful tool for monitoring crop condition, biomass, and productivity across multiple scales (Xiao et al., 2006; Nemani et al., 2003). Sensors including MODIS, INSAT-3D, and Sentinel-2 provide frequent, synoptic data on canopy reflectance, photosynthetically active radiation, vegetation indices, and surface temperature—parameters directly linked to crop growth (Gitelson et al., 2015; Pinker &Frouin, 1995).

A range of modelling approaches has been designed to convert remotely sensed data into quantitative yield estimates. Empirical regression models use vegetation indices to infer yield (Prince et al., 1998), while complex process-based crop growth models simulate detailed plant-environment interactions (Running & Coughlan, 1988; Prentice et al., 1992). However, empirical models may not generalise well across seasons and locations, and mechanistic models require extensive parameterisation and site-specific inputs (Moulin et al., 1998).

To address these limitations, semi-physical approaches have gained prominence. Rooted in Monteith's (1982) light-use efficiency theory, these models integrate process understanding with satellite-derived biophysical variables. Their central principle is the estimation of Net Primary Productivity (NPP) through the combination of incident Photosynthetically Active Radiation (PAR), the Fraction of PAR absorbed by vegetation (fAPAR), and Radiation Use Efficiency (RUE), with modifiers for temperature and water stress (Jia et al., 2020; Moulin et al., 1998; Wang et al., 2019). Grain yield is then obtained by applying a harvest index (Potter et al., 1993; Prince &Goward, 1995). Such semi-physical NPP frameworks have been widely tested for major crops-wheat (Tripathy et al., 2014), sugarcane (Chaurasiya et al., 2017), maize (Gitelson et al., 2015), and rice (Jia et al., 2020; Dwivedi et al., 2019; Yang et al., 2018)and consistently demonstrate reliable performance when validated with field data.

The global value of semi-physical models is underscored by research linking vegetation productivity and carbon balance to climate dynamics. Studies have highlighted how photosynthesis and ecosystem growth are modulated by climatic drivers (Beer et al., 2010; Myneni et al., 1997; Liu et al., 2017), while other work shows how land-use change and warming trends reshape vegetation productivity (Houghton, 1999; Nemani et al., 2001; Feng et al., 2016; Pan et al., 2011).

Bhandara District, situated in the eastern Vidarbha region of Maharashtra, offers an ideal setting for operational yield modelling. Known as the 'rice bowl' of Maharashtra, its fertile alluvial plains, sustained by the Wainganga River, are extensively cultivated with paddy, whereas nearby uplands often experience water stress and soil erosion. Agriculture in the district is increasingly challenged by erratic monsoon rainfall, rising temperatures, and land-use pressures (Feng et al., 2016; Houghton, 1999; Nemani et al., 2003). Developing spatially explicit yield forecasts for this landscape is therefore vital for optimising irrigation and fertiliser use, managing resources, and reducing risk.

Several investigations have shown that combining PAR from geostationary satellites with fAPAR and vegetation indices from MODIS, and incorporating temperature or moisture stress indicators, can substantially improve rice yield prediction (Gitelson et al., 2015; Moulin et al., 1998; Wang et al., 2019). The use of high-resolution crop masks from Sentinel-2 or radar data enhances discrimination of rice fields and improves the precision of pixel-level yield estimates (Xiao et al., 2006; Chaurasiya et al., 2017).

Against this background, the present study develops and evaluates a semi-physical remote sensing framework for paddy yield estimation in Bhandara District during the 2018-2022 kharif seasons. The framework incorporates PAR (0.4-0.7 μm), fAPAR, RUE, and stress factors for temperature and water within an NPP model (Kumar & Monteith, 1982; Jia et al., 2020; Moulin et al., 1998), and validates the derived yields against official crop-cutting statistics. By combining crop growth models with remotely sensed information, the research aims to overcome the

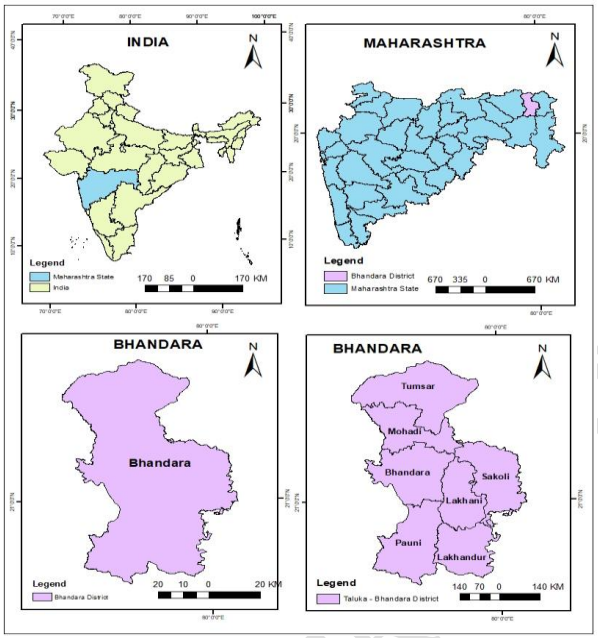

limitations of yield prediction at regional scales. The findings offer significant potential for guiding farmers' decision-making, improving paddy management, and informing evidence-based agricultural policy across Maharashtra and other rice-growing regions.

Fig. 1. Map showing the location of study area

2. MATERIAL AND METHODS:

Data Sources:

A variety of satellite and ground-based datasets were used to drive the semi-physical yield estimation model (Table 1). Daily photosynthetically active radiation (PAR) was derived from INSAT-3D insolation data (4 km resolution, obtained from MOSDAC). Fraction of absorbed PAR (fAPAR) was obtained as a 10-day composite from Terra-MODIS (500 m), and MODIS surface reflectance data were used to generate Land Surface Water Index (LSWI). A theme of paddy crop mask was developed from Sentinel-2 imagery (10 m) acquired from ESA Copernicus. Daily temperature data were sourced from Skymet and NASA POWER, while harvest index values were derived from crop-cutting experiments (CCE) reported by the Department of Agriculture, Maharashtra. The data processing was carried out using ArcGIS, ERDAS Imagine, and uR Studio.

Comment [H1]: Present in Materials and Methods

Comment [H2]: Provide reference

Comment [H3]: Check Table No

Comment [H4]: The weather

Comment [H5]: Reference

Methodology:

The estimation of rice yield was carried out using a semi-physical approach that integrates satellite-derived biophysical parameters with crop-specific constants. Photosynthetically Active Radiation (PAR) was first computed from daily insolation data obtained from INSAT-3D, which were aggregated into an 8-day composite for the entire crop season. Fifty percent of the incoming solar radiation, corresponding to the 0.4-0.7 µm wavelength range, was assumed to represent PAR, following the relation PAR = Insolation(8-day) × 0.5.

The fraction of absorbed PAR (fAPAR) was retrieved from MODIS 10-day composite products. Physical values ranging from 0 to 1 were extracted from digital numbers through appropriate scaling, allowing the representation of canopy photosynthetic efficiency over time. Radiation use efficiency (RUE), denoted as ε, was assumed constant at 2.3 g MJ^{-1}, consistent with values reported in the literature for paddy crops.

Temperature stress (T stress) was derived from daily mean air temperature data acquired from NASA POWER and Skymet. It was calculated using thresholds specific to rice photosynthesis, namely a minimum temperature (T min) of 14 °C, a maximum temperature (T max) of 40 °C, and an optimum temperature (T opt) of 30 °C. The stress scalar was expressed as:

T stress = ((T –T min) (T –T max)) / ((T –T min) (T –T max) - (T –T opt)²),
and was set to zero whenever T <T min.

Similarly, Water stress (W stress) was estimated from the Land Surface Water Index (LSWI), computed using MODIS surface reflectance bands as:

LSWI = (ρNIR-ρSWIR) / (ρNIR + ρSWIR),

where ρNIR and ρSWIR represent the near-infrared and shortwave infrared reflectances, respectively. The maximum value of LSWI (LSWImax) observed across the paddy mask was used to normalize the water stress component as:

W stress = (LSWI -LSWImin) / (LSWImax-LSWImin).

A paddy crop mask was generated using Sentinel-2 imagery acquired between July and October 2022. Supervised classification in ERDAS Imagine identified paddy fields, while temporal vegetation index profiles were analyzed to characterize sowing dates, transplanting periods, and phenological stages.

Net Primary Productivity (NPP) was estimated using the Monteith (1972) model:

NPP = PAR × fAPAR × ε × Tstress × Wstress.

Comment [H6]: Reference

Comment [H7]: The arbitrary

Comment [H8]: Reference

Comment [H9]: During kharif season between

Finally, a harvest index (HI) of 0.50, derived from crop-cutting experiments, was applied to convert NPP into grain yield according to:

Grain Yield = NPP × HI.

The methodological framework allowed for the integration of remotely sensed data, meteorological inputs, and crop parameters to estimate spatially explicit rice yield across Bhandara district.

3. RESULTS AND DISCUSSION:

3.1 Photosynthetic Absorbed Radiation (PAR):

Comment [H10]: Active

Photosynthetically Active Radiation (PAR) represents the portion of incoming solar energy in the 0.4-0.7 µm spectral range that is available for photosynthesis. For this study, PAR was derived from daily insolation data obtained from the INSAT-3D sensor via the MOSDAC data portal (https://www.mosdac.gov.in). Daily values were aggregated into 8-day composites to reduce noise and capture the seasonal signal, and 50 % of the incident solar radiation was assumed to constitute PAR, following standard practice (PAR = 0.5 × 8-day insolation).

Comment [H11]: Delete District, Crop, Season, Place North arrow in up word corner, convert legend to annotation/graphics, keep only PAR and their value in all the theme maps

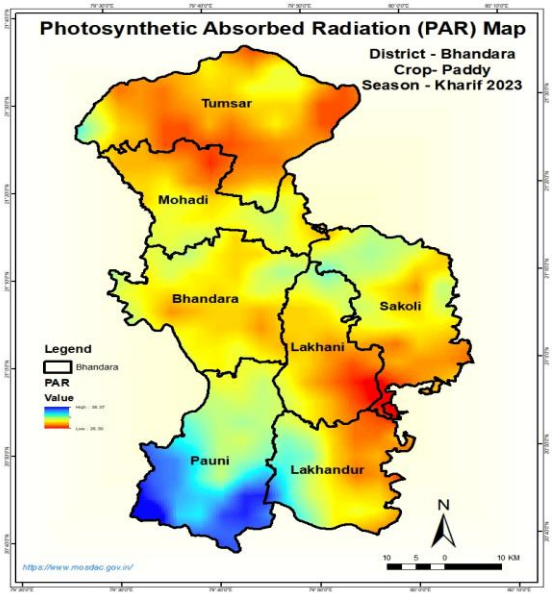

Fig. 2. Photosynthetically Active Radiation (PAR) distribution across Bhandara District for the kharif 2023 paddy season

PAR values range from 26.5 to 38.4 MJ m^{-2}, with higher levels observed in the northern and central talukas, Tumsar, Mohadi, and parts of Lakhan indicating greater availability of photosynthetically useful energy in these areas (Fig. 2). Moderate PAR occurs in Sakoli, Lakhani, and Lakhundar, while the lowest levels (<28 MJ m^{-2}) are concentrated in the southern taluka of Pauni. The observed gradient likely reflects a combination of latitudinal position, local cloud cover, and micro-climatic conditions during the season.

Spatial variability in PAR is an important driver of crop growth because it governs the amount of radiant energy available for canopy photosynthesis. Areas receiving consistently high PAR are expected to support higher Net Primary Productivity (NPP) when other factors such as soil moisture and temperature remain favourable. Conversely, the relatively low PAR recorded over Pauni and neighbouring areas suggests a potential constraint on biomass accumulation and yield if not compensated by improved agronomic or climatic conditions. These findings highlight the importance of accurately quantifying the radiation component in semi-physical yield models, as even moderate spatial differences can lead to significant variation in predicted grain yield.

The areas of higher PAR is suitable for long duration varieties followed by medium and short duration varieties in moderate PAR values.

3.2 Fraction of Absorbed Photosynthetically Active Radiation (FAPAR):

Fraction of Absorbed Photosynthetically Active Radiation (FAPAR) is a key biophysical variable describing the proportion of incoming PAR that is intercepted and absorbed by green vegetation. For this study, FAPAR was obtained from the MODIS 10-day composite product (1 km resolution), with physical values retrieved from the sensor's digital numbers. The index ranges between 0 (no absorption) and 1 (complete absorption), reflecting canopy density and photosynthetic potential.

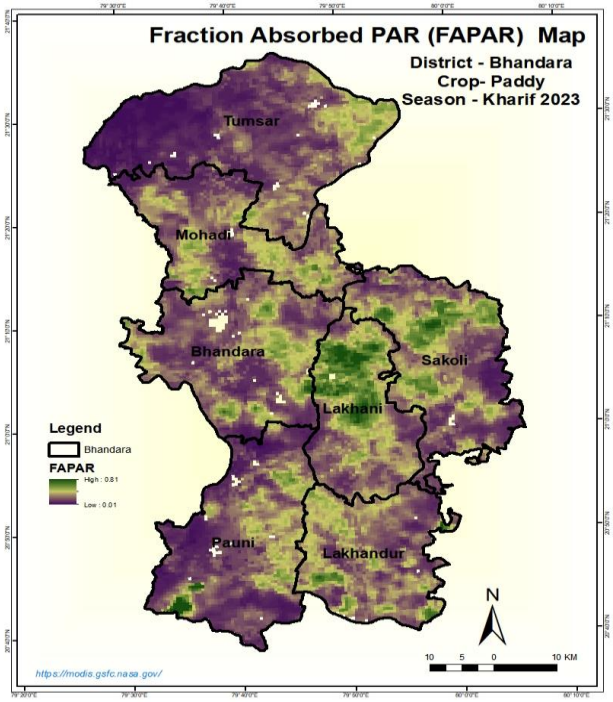

Fig. 3. Spatial distribution of the FAPAR across Bhandara District for the kharif 2023 paddy season

Values of FAPAR across Bhandara District for the kharif 2023 paddy season range from 0.01 to 0.81, indicating pronounced heterogeneity in canopy development (Fig. 3). The highest FAPAR levels (>0.70) occur in parts of Lakhani, Sakoli, and scattered patches of Mohadi and Bhandara talukas, suggesting dense, actively photosynthesising paddy crop. Moderate values (0.40-0.60) dominate central areas, while low absorption (<0.20) is evident over Pauni, Tumsar, and some upland zones, likely reflecting sparse vegetation, early growth stages, or water-limited fields (Fig. 3).

Comment [H12]: May not suitable for paddy cultivation

The observed variability corresponds well with differences in crop establishment, soil moisture, and microclimatic conditions within the district. Areas with higher FAPAR are expected to contribute more strongly to Net Primary Productivity (NPP), supporting greater biomass accumulation and potential yield. Conversely, low FAPAR regions may require targeted agronomic interventions such as improved transplanting practices or supplemental irrigation to enhance canopy vigour and productivity. The spatial characterisation of FAPAR thus provides an essential input to the semi-physical NPP model, enabling more accurate yield estimation at the taluka level.

3.3 Temperature Stress (Tstress):

Temperature stress is a critical factor influencing the growth, photosynthetic efficiency, and grain-filling stages of paddy crops. For the present study, daily average temperature data were acquired from the NASA POWER database (https://power.larc.nasa.gov/data-access-viewer.html) at a spatial resolution of 1° × 1°. Temperature stress (Tstress) was computed using threshold parameters for paddy growth: minimum temperature (Tmin) = 14 °C, maximum temperature (Tmax) = 40 °C, and optimum temperature (Topt) = 30 °C. These limits represent the physiological tolerance range within which rice performs best, while departures from these values reduce photosynthetic activity and biomass accumulation.

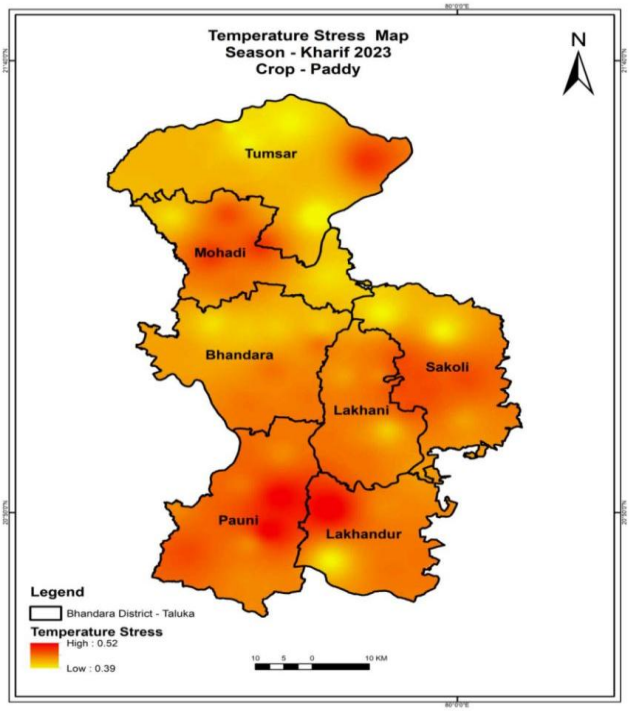

Fig. 4. Spatial distribution of temperature stress (Tstress) for paddy during the kharif 2023 season

Tstress values range between 0.39 and 0.52**,** with higher stress (≥0.50) observed over Pauni, parts of Lakhani, and scattered pockets in Tumsar and Sakoli (Fig. 4). These areas indicate sub-optimal thermal conditions, likely linked to short episodes of elevated temperature or persistent warm nights during sensitive crop stages. Moderate stress values dominate most of Mohadi, Bhandara, and Lakhundar, suggesting generally favourable thermal regimes with occasional heat constraints.

Comment [H13]: Observed in the ridges of the study area, which may not suitable for paddy cultivation.

Spatial variability in Tstress underscores the influence of microclimatic differences, such as altitude, proximity to water bodies, and local cloud cover, on paddy performance. Elevated temperature stress may accelerate crop senescence, shorten the grain-filling period, and reduce yield potential, whereas areas with lower stress values are expected to sustain higher Net

Primary Productivity (NPP) and better grain formation. The map provides essential input for the semi-physical yield model, allowing accurate representation of temperature limitations on rice productivity.

3.4 Land Surface Water Index (LSWI)

The Land Surface Water Index (LSWI) is a spectral indicator derived from the near-infrared (NIR) and short-wave infrared (SWIR) reflectance bands of satellite data. It is sensitive to vegetation moisture content and surface water presence, making it a useful proxy for paddy field wetness and crop water stress.

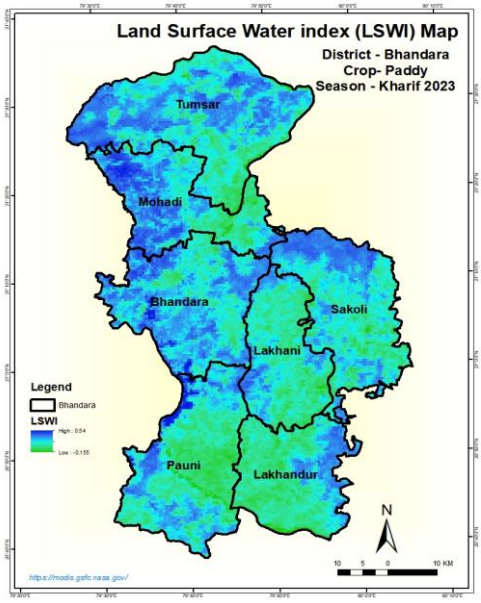

Fig. 5. Spatial distribution of the Land Surface Water Index (LSWI) for the kharif 2023 paddy season

The values range of LSWI across Bhandara District from -0.155 to 0.54, with higher positive values indicating abundant surface or soil moisture and lower values reflecting drier conditions or sparse vegetation. Elevated LSWI (>0.40) is evident in extensive parts of Lakhani, Lakhundar, and Pauni, signifying low lands, well-watered paddy fields and favourable hydrological conditions during the crop's vegetative phase. Moderate values (0.20-0.35) occur in Bhandara, Mohadi, and Sakoli, whereas relatively low LSWI (<0.10) is observed in pockets of

Tumsar and upland margins, suggesting limited standing water or early onset of moisture stress (Fig. 5).

The spatial heterogeneity of LSWI corresponds to variations in irrigation coverage, rainfall distribution, and soil water retention across the district. Areas with consistently high LSWI are expected to maintain optimal plant water status, supporting higher photosynthetic activity and biomass production, while lower values highlight locations where supplementary water management may be necessary. As a component of the semi-physical yield model, LSWI contributes to estimating water stress (Wstress) and thus enhances the reliability of Net Primary Productivity (NPP) and grain yield assessments.

3.5 Water Stress (Wstress):

Water stress is a key determinant of crop growth and yield, reflecting the availability of soil and surface moisture relative to plant requirements.

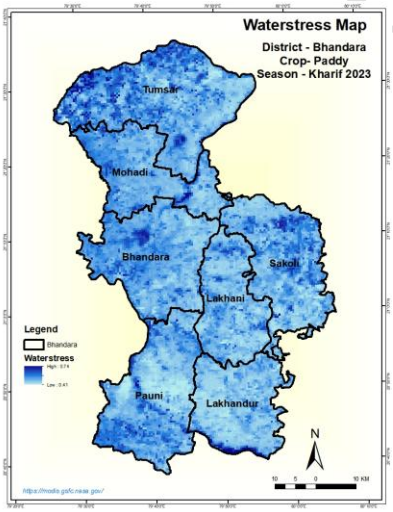

Fig. 6. Spatial distribution of water stress (Wstress) for paddy in Bhandara District

Fig. 6 depicts the spatial distribution of Wstress in Bhandara District for the 2023 kharif paddy crop. Values range between 0.41 and 0.74, with higher values denoting greater moisture stress. Moderate to elevated stress (>0.65) is evident in parts of Pauni, Lakhundar, and isolated zones of Mohadi and Bhandara, indicating potential limitations in soil water availability during critical growth phases. Conversely, lower stress levels (<0.50) prevail across Lakhani, Sakoli, and

the central belt, signifying adequate surface or soil moisture and favourable conditions for crop development.

The distribution pattern reflects the interplay of rainfall variability, irrigation access, and soil water-holding capacity within the district. Areas with high water stress correspond to locations where rainfall may have been uneven or irrigation infrastructure is sparse, while low-stress regions likely benefit from better hydrological support. Quantifying Wstress provides essential input to the semi-physical yield model by constraining Net Primary Productivity (NPP) estimates, ensuring that simulated biomass and yield reflect the actual water regime experienced by the crop.

3.6 Crop Classification of Paddy:

Accurate delineation of paddy areas is fundamental for yield estimation, as it enables the spatial integration of biophysical parameters and stress indices with crop extent. In this study, a paddy crop mask for Bhandara District was generated from Sentinel-2 imagery using supervised classification in ERDAS Imagine.

Comment [H14]: Time of Image downloaded

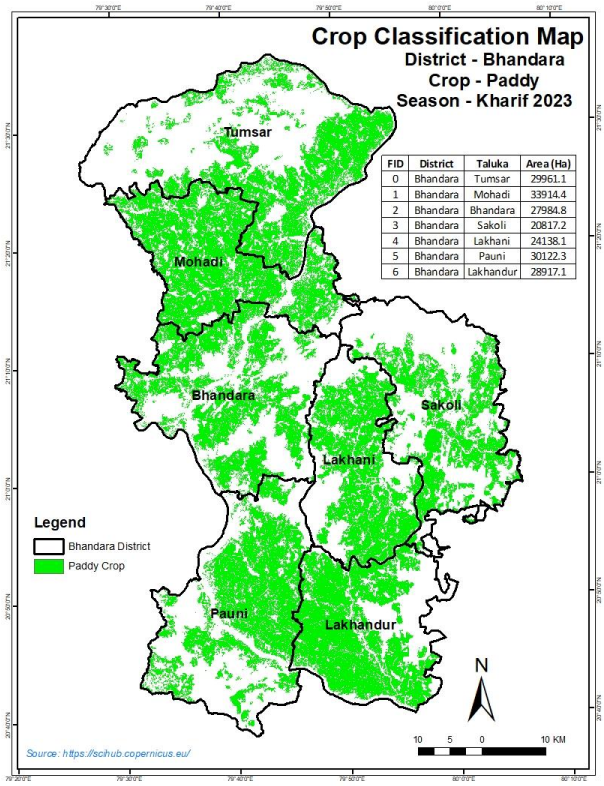

FID	District	Taluka	Area (Ha)
0	Bhandara	Tumsar	29961.1
1	Bhandara	Mohadi	33914.4
2	Bhandara	Bhandara	27984.8
3	Bhandara	Sakoli	20817.2
4	Bhandara	Lakhani	24138.1
5	Bhandara	Pauni	30122.3
6	Bhandara	Lakhandur	28917.1

Fig. 7. Classified paddy distribution for the kharif 2023 season in Bhandara District

The classified paddy distribution map reveals a widespread concentration of paddy fields across all talukas, with particularly dense coverage in Mohadi (33,914.4 ha), Pauni (30,122.3 ha), and Tumsar (29,961.1 ha). Substantial areas are also observed in Lakhundar (28,917.1 ha), Bhandara (27,984.8 ha), and Sakoli (20,817.2 ha), while Lakhani (24,138.1 ha) shows moderate but well-distributed coverage (Fig. 7). These figures confirm the predominance of rice cultivation throughout the district, highlighting its role as the “rice bowl” of Maharashtra.

Comment [H15]: Compare with the total area and per cent area of paddy contributing

The spatial distribution illustrates a mosaic of continuous and fragmented paddy patches, reflecting differences in landholding patterns, irrigation availability, and terrain. Low-lying floodplains and gently sloping valley bottoms support larger contiguous fields, whereas upland fringes contain smaller, scattered plots. The classified map provides an essential baseline for overlaying PAR, FAPAR, temperature, and water stress layers, enabling precise calculation of Net Primary Productivity (NPP) and grain yield at the taluka and pixel levels.

3.7 Sowing Dates and Crop Growth Profile:

Table 1. Temporal profile of sowing dates and canopy growth for ten representative paddy field classes

Date	Class 1	Class 2	Class 3	Class 4	Class 5	Class 6	Class 7	Class 8	Class 9	Class 10
4 July	0.23	0.33	0.44	0.46	0.36	0.27	0.37	0.40	0.41	0.41
12 July	0.06	0.07	0.08	0.09	0.09	0.08	0.09	0.10	0.12	0.08
20 July	0.21	0.18	0.22	0.20	0.30	0.48	0.40	0.37	0.30	0.55
28 July	0.11	0.15	0.14	0.16	0.13	0.11	0.14	0.15	0.18	0.14
5 August	0.52	0.54	0.42	0.62	0.48	0.51	0.59	0.57	0.60	0.64
13 August	0.50	0.63	0.58	0.62	0.45	0.51	0.59	0.59	0.66	0.64
21 August	0.64	0.68	0.59	0.66	0.45	0.67	0.64	0.63	0.69	0.64
29 August	0.76	0.80	0.75	0.78	0.70	0.78	0.77	0.75	0.80	0.77
6 September	0.17	0.17	0.18	0.23	0.17	0.17	0.20	0.18	0.19	0.23
14 September	0.77	0.87	0.80	0.69	0.60	0.73	0.33	0.77	0.85	0.70
22 September	0.78	0.69	0.82	0.82	0.67	0.83	0.77	0.47	0.83	0.79
30 September	0.79	0.74	0.78	0.76	0.68	0.78	0.75	0.76	0.76	0.74
8 October	0.78	0.69	0.76	0.73	0.66	0.76	0.73	0.73	0.71	0.71
16 October	0.72	0.52	0.67	0.61	0.58	0.67	0.62	0.63	0.57	0.59
24 October	0.67	0.45	0.61	0.56	0.53	0.62	0.57	0.58	0.50	0.54
1 November	0.54	0.37	0.52	0.47	0.45	0.50	0.47	0.49	0.42	0.45
9 November	0.51	0.37	0.49	0.46	0.44	0.48	0.46	0.48	0.42	0.45
17 November	0.45	0.38	0.45	0.44	0.44	0.44	0.44	0.45	0.41	0.43
25 November	0.43	0.39	0.44	0.43	0.43	0.44	0.44	0.45	0.42	0.43

Table 1 summarises the temporal evolution of canopy development for ten representative paddy field classes in Bhandara District during the *kharif* 2023 season. The values represent vegetation response (e.g., NDVI/FAPAR-like scores) extracted from time-series satellite observations, reflecting crop establishment, growth dynamics, and senescence.

The data indicate that transplanting or sowing activities commenced in early July, with modest canopy values recorded on 4 July (0.23-0.46 across classes). By 12 July**,** indices declined slightly, suggesting either the persistence of standing water or delayed transplanting in

some plots. From 20 July onwards, values began to increase, marking the onset of seedling establishment and early vegetative growth.

A pronounced rise was observed between 5 and 29 August, when values exceeded 0.50 across most classes and peaked at 0.80 in several locations. This period coincides with the rapid vegetative phase, characterised by active tillering and canopy expansion under favourable monsoon conditions. By late August, most classes exhibited values between 0.70 and 0.80, indicating dense, photosynthetically active stands approaching their maximum leaf area (Table 1).

Following peak greenness, a gradual decline occurred from 6 September, interrupted by a brief rebound around 14-22 September, possibly reflecting panicle initiation and grain-filling in well-managed fields. After 30 September, indices steadily decreased, indicating the onset of maturity and senescence. By 19 November, values had fallen to approximately 0.42-0.54, and by 25 November they stabilised near 0.43, representing post-harvest residue or bare soil (Table 1).

Spatial differences among the ten classes suggest variability in sowing dates, water availability, or cultivar choice. Early-maturing areas (e.g., Classes 1-4) reached peak canopy earlier, while Classes 8-10 maintained higher values into October, consistent with later transplanting or longer-duration varieties.

Overall, the growth profile demonstrates a typical rice phenological cycle in monsoon ecosystems: transplanting in early July, vigorous vegetative growth in August, reproductive and ripening phases during September-October, and harvest completion by late November. This temporal characterisation is critical for parameterising semi-physical yield models, scheduling crop management interventions, and validating satellite-based productivity assessments.

3.8 Biomass (Net Primary Productivity):

Net Primary Productivity (NPP) represents the net accumulation of carbon in plant biomass and is a direct indicator of crop growth and productivity. For this study, NPP was computed using the semi-physical light-use efficiency model, integrating Photosynthetically Active Radiation (PAR), Fraction of Absorbed PAR (FAPAR), Radiation Use Efficiency (RUE), and stress scalars for temperature and water over the *kharif* 2023 season (July–November). The resulting biomass values, expressed in g C m^{-2}, provide a spatially explicit measure of paddy growth across Bhandara District.

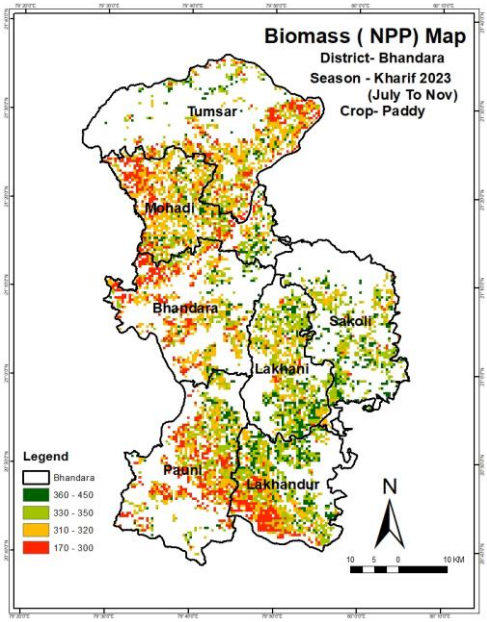

Fig. 8. Spatial distribution of Net Primary Productivity (NPP) for paddy in Bhandara District during the kharif 2023 season (July–November).

Fig. 8 illustrates the distribution of NPP for the 2023 paddy crop. Biomass values range from 170 to 450 g C m^{-2}, with the highest productivity (360-450 g C m^{-2}) concentrated in the talukas of Lakhani, Sakoli, and parts of Mohadi, where favourable radiation, moisture, and temperature conditions supported optimal photosynthetic activity. Moderate biomass (330-350 g C m^{-2}) is observed across Bhandara, Lakhundar, and sections of Pauni, reflecting adequate but not peak growing conditions. Lower NPP values (170-300 g C m^{-2}) dominate the upland fringes of Pauni, western Mohadi, and isolated patches in Tumsar, indicating growth constraints possibly linked to moisture stress, late transplanting, or suboptimal nutrient management.

The spatial variability in NPP mirrors the combined influence of environmental factors and management practices, emphasising the importance of accounting for radiation, water, and thermal regimes when estimating crop biomass. High-NPP zones align closely with areas of low temperature and water stress, while regions of reduced biomass correspond to elevated stress indices and less favourable canopy vigour. This analysis provides a valuable basis for identifying yield gaps, targeting agronomic interventions, and validating grain yield estimates derived from the NPP model.

3.9 Grain Yield Estimation:

Grain yield for the *kharif* 2023 paddy crop in Bhandara District was estimated by applying a harvest index (HI = 0.50) to Net Primary Productivity (NPP) derived from the semi-physical light-use efficiency model. The resulting spatial yield estimates, expressed in kg ha^{-1}, are shown in Fig. 9.

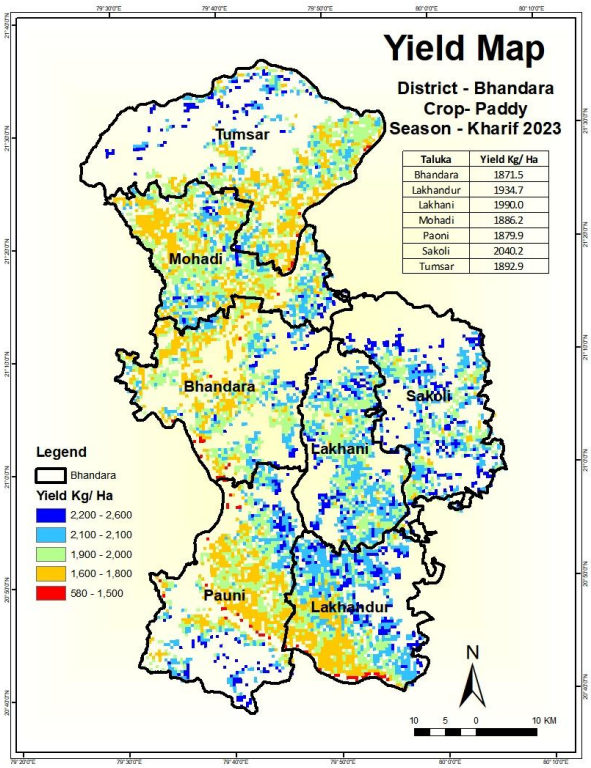

Fig. 9. Spatial distribution of estimated paddy grain yield (kg ha^{-1}) in Bhandara District for the kharif 2023 season.

Yields range from **580 to 2,600 kg ha^{-1}**, displaying considerable heterogeneity across the district. The highest yields (2,200–2,600 kg ha^{-1}) occur in parts of Sakoli, Lakhani, and central Lakhundar, reflecting optimal canopy vigour, favourable radiation use, and adequate soil moisture. Moderately high yields (2,000-2,100 kg ha^{-1}) are distributed across Mohadi, Tumsar, and pockets of Pauni, whereas intermediate yields (1,600-1,900 kg ha^{-1}) dominate the western portions of Bhandara and upland zones of Pauni and Mohad (Fig. 9).

Lower yields (<1,500 kg ha^{-1}) are scattered in the southern and western fringes, particularly in Pauni and sections of Lakhundar, coinciding with areas that experienced higher

Comment [H16]: Classify the land for marginal/productive land by super imposing drainage layer. The drainage layer provide clue for classifying low land which are highly productive for paddy cultivation.

water or temperature stress, or possibly delayed transplanting and suboptimal nutrient management. The taluka-wise averages presented in the inset table further highlight Sakoli (2,040.2 kg ha^{-1}) and Lakhani (1,990 kg ha^{-1}) as the best-performing areas, while Bhandara (1,871.5 kg ha^{-1}) and Pauni (1,879.9 kg ha^{-1}) show moderate productivity.

The observed spatial variability underscores the influence of local environmental conditions, irrigation access, and agronomic practices on paddy performance. Integrating such yield maps with stress indicators can help prioritise regions for agronomic support and guide precision farming interventions to reduce yield gaps and enhance food security.

4. CONCLUSION

This study applied a semi-physical remote sensing framework to estimate paddy yield in Bhandara District, Maharashtra, during the *kharif* 2023 season. By combining Photosynthetically Active Radiation (PAR), Fraction of Absorbed PAR (FAPAR), Radiation Use Efficiency (RUE), and stress scalars for temperature and water within a Net Primary Productivity (NPP) model, detailed spatial patterns of biomass and grain yield were derived.

The analysis revealed clear gradients in biophysical conditions across the district. PAR and FAPAR showed strong variability between northern, central, and southern talukas, reflecting differences in radiation availability, canopy vigour, and local weather. Water and temperature stress maps highlighted areas where suboptimal moisture or excessive heat constrained crop performance, while LSWI confirmed favourable water status in irrigated and low-lying fields. The crop growth profile captured a typical rice phenological cycle, from early transplanting in July, through vigorous vegetative development in August, reproductive and ripening stages in September-October, and senescence by late November.

Biomass (NPP) estimates ranged from 170 to 450 g C m^{-2}**,** with the highest values in Lakhani, Sakoli, and Mohadi, and lower productivity in upland zones of Pauni and western Mohadi. Yield predictions, derived from NPP using a harvest index, varied from 580 to 2,600 kg ha^{-1}**,** with superior yields in Sakoli, Lakhani, and parts of Lakhundar, and modest outputs in Pauni and fringe areas. These spatial patterns underscore the importance of radiation, canopy density, water status, and temperature regimes in shaping paddy productivity.

The findings highlight that remote sensing–based semi-physical models can complement conventional crop assessment methods, offering a timely, cost-effective, and objective alternative for monitoring paddy performance over heterogeneous landscapes. Beyond yield estimation, the derived stress indices (temperature and water) provide actionable insights for identifying vulnerability hotspots and guiding resource allocation, irrigation scheduling, and fertiliser management.

Overall, the research demonstrates that integrating Earth-observation data with a light-use efficiency model offers a robust and cost-effective approach for mapping biomass and yield at field-to-district scales. The resulting information can support sitespecific management**,** irrigation planning, and strategic interventions aimed at reducing yield gaps and enhancing rice production sustainability in Bhandara and similar agro-ecological settings. Future efforts should focus on incorporating finer-resolution sensors and multi-year datasets to capture crop response under varying climatic and management conditions.

DISCLAIMER (ARTIFICIAL INTELLIGENCE)

Authors hereby declare that no generative AI technologies such as Large Language Models (ChatGPT, COPILOT, etc.) and text-to-image generators have been used during writing or editing of this manuscript.

REFERENCES

Beer, C., Reichstein, M., Tomelleri, E., Ciais, P., Jung, M., Carvalhais, N., ... &Papale, D. (2010). Terrestrial gross carbon dioxide uptake: global distribution and covariation with climate. Science, 329(5993), 834-838.

Begue, A., Bégué, A., &Zoungrana, B. J. B. (2010). "Near real-time monitoring of crop productivity using remote sensing." Sensors, 10(6), 5045-5069. DOI: 10.3390/s100605045.

25. Feng, X., Fu, B., Piao, S., Wang, S., Ciais, P., Zeng, Z., ... & Myneni, R. (2016). Revegetation in China's Loess Plateau is approaching sustainable water resource limits. Nature Climate Change, 6(11), 1019-1022.

https://www.globalforestwatch.org/dashboards/country/ ND/4/?category=summary&location

G. Chaurasiya, Shalini Saxena*, RojalinTripathy**, K. N. Chaudhari ** and S. S. Ray* “Semi Physical Approach for Sugarcane Yield Modelling with Remotely Sensed Inputs” Vayu Mandal 43(1), 2017.

Gitelson, A. A., Peng, Y., &Arkebauer, T. J. (2015). Relationships between gross primary production, green LAI, and canopy chlorophyll content in maize: implications for remote sensing of primary production. Remote Sensing of Environment, 156, 96-106.

19. Houghton, R. A. (1999). The annual net flux of carbon to the atmosphere from changes in land use 1850-1990. Tellus B: Chemical and Physical Meteorology, 51(2), 298-313.

Jia, L., Li, C., Wang, L., & Chen, H. (2020). A Semi-Physical Model for Estimating Rice Yield Using Remote Sensing Data and Meteorological Information. Remote Sensing, 12(7), 1176.

Liu, J., Bowman, K. W., Schimel, D. S., Parazoo, N. C., Jiang, Z., Lee, M., ... &Gierach, M. M. (2017). Contrasting carbon cycle responses of the tropical continents to the 2015-2016 El Niño. Science, 358(6360), eaam5690.

Ma, S., Zhu, Y., Li, Y., & Liu, Q. (2018). Estimating Crop Yield Based on Net Primary Productivity (NPP) Derived from Remote Sensing Data: A Case Study of Wheat in China. Remote Sensing, 10(7), 1049.

Manish Dwivedi *, Shalini Saxena, Neetu and S. S. Ray, "ASSESSMENT OF RICE BIOMASS PRODUCTION AND YIELD USING SEMIPHYSICAL APPROACH AND REMOTELY SENSED DATA" The International Archives of the Photogrammetry, Remote Sensing and Spatial Information Sciences, Volume XLII-3/W6, 2019.

Moran, M. S., Clarke, T. R., Inoue, Y., & Vidal, A. (1995). "Estimating crop water deficit using the relation between surface-air temperature and spectral vegetation index." Remote Sensing of Environment, 49(3), 246-263. DOI: 10.1016/0034-4257(94)00084-L

Moulin, S., Trottet, M., Faivre, R., &Ceccato, P. (1998). "A regional crop model using a satellite-derived index for water stress." Agricultural and Forest Meteorology, 91(1-2), 51-63. DOI: 10.1016/S0168-1923(98)00069-3.

Monteith, J. L. (1982). Solar radiation and productivity in tropical ecosystems. Journal of Applied Ecology, 19(3), 657-666.

Myneni, R. B., Keeling, C. D., Tucker, C. J., Asrar, G., &Nemani, R. R. (1997). Increased plant growth in the northern high latitudes from 1981 to 1991. Nature, 386(6626), 698-702.

Nemani, R. R., Keeling, C. D., Hashimoto, H., Jolly, W. M., Piper, S. C., Tucker, C. J., ... & Running, S. W. (2003). Climate-driven increases in global terrestrial net primary production from 1982 to 1999. Science, 300(5625), 1560-1563.

Nemani, R. R., White, M. A., Cayan, D. R., Jones, G. V., Running, S. W., & Coughlan, J. C. (2001). Asymmetric warming over coastal California and its impact on the premium wine industry. Climate Research, 19(1), 25-34.

Pan, Y., Birdsey, R. A., Fang, J., Houghton, R., Kauppi, P. E., Kurz, W. A., ... & Woodall, C. W. (2011). A large and persistent carbon sink in the world's forests. Science, 333(6045), 988-993.

Potter, C. S., Randerson, J. T., Field, C. B., Matson, P. A., Vitousek, P. M., Mooney, H. A., &Klooster, S. A. (1993). Terrestrial ecosystem production: A process model based on global satellite and surface data. Global Biogeochemical Cycles, 7(4), 811-841.

Prince, S. D., Brown De Colstoun, E., & Kravitz, L. L. (1998). Evidence from rain-use efficiencies does not indicate extensive Sahelian desertification. Global Change Biology, 4(3), 359-374.

Prentice, I. C., Cramer, W., Harrison, S. P., Leemans, R., Monserud, R. A., & Solomon, A. M. (1992). A global biome model based on plant physiology and dominance, soil properties and climate. Journal of Biogeography, 19(2), 117-134.

Pinker, R. T., &Frouin, R. (1995). "Estimation of daily photosynthetically available radiation from satellite observations." Journal of Applied Meteorology, 34(12), 2797-2822. DOI: 10.1175/1520-0450(1995)034<2797: eodpar>2.0.co;2.

Prince, S. D., &Goward, S. N. (1995). Global primary production: A remote sensing approach. Journal of Biogeography, 22(5), 815-835.

R Tripathy a, *, K.N. Chaudhary a, R.Nigam a, K.R. Manjunath a, P. Chauhan a, S.S. Ray b, and J.S. Parihar a .OPERATIONAL SEMI-PHYSICAL SPECTRAL-SPATIAL WHEAT YIELD MODEL DEVELOPMENT, 10.5194/isprsarchives-XL-8-977-2014.

Running, S. W., & Coughlan, J. C. (1988). A general model of forest ecosystem processes for regional applications I. Hydrologic balance, canopy gas exchange and primary production processes. Ecological Modelling, 42(2-4), 125-154.

Wang, X., Wang, H., & Zhang, J. (2019). Integrating Remote Sensing and NPP Models for Accurate Crop Yield Estimation in Complex Agricultural Landscapes. Agricultural and Forest Meteorology, 272-273, 83-92.

Xiao, X., Boles, S., Frolking, S., Li, C., Babu, J. Y., Salas, W., & Moore III, B. (2006). Mapping paddy rice agriculture in South and Southeast Asia using multi-temporal MODIS images. Remote Sensing of Environment, 100(1), 95-113.

Yang, W., Liu, Q., Zhang, X., Chen, J., Zhang, Y., & Wang, J. (2018). Estimation of Net Primary Productivity Using MODIS Data and Model in Northeast China, 2001–2015. Remote Sensing, 10(6), 886.

Yao, Y., Li, Z., Tian, F., & Tao, F. (2021). Remote Sensing-Based Estimation of Maize Yield Using a Semi-Physical Approach: A Case Study in the North China Plain. Frontiers in Plant Science, 12, 662.

Zhou, G., Wu, X., Meng, Z., Zhou, C., Wang, Y., & Shi, P. (2003). "Evaluation of the photosynthetic productivity of terrestrial vegetation from MODIS data using a modified Farquhar model." Remote Sensing of Environment, 84(2), 149-162. DOI: 10.1016/S0034-4257(02)00137-3.

Zhao, M., & Running, S. W. (2010). Drought-induced reduction in global terrestrial net primary production from 2000 through 2009. Science, 329(5994), 940-943.